

# Probing the spin-glass phase with non-equilibrium measurements: statics-dynamics equivalence through the fluctuation-dissipation ratio

M. Baity-Jesi,<sup>1</sup> E. Calore,<sup>2</sup> A. Cruz,<sup>3,4</sup> L.A. Fernandez,<sup>5,4</sup> J.M. Gil-Narvion,<sup>4</sup> A. Gordillo-Guerrero,<sup>6,4</sup> D. Iñiguez,<sup>4,7</sup> A. Maiorano,<sup>8,4</sup> E. Marinari,<sup>8,9</sup> V. Martin-Mayor,<sup>5,4</sup> J. Monforte-Garcia,<sup>4</sup> A. Muñoz-Sudupe,<sup>5,4</sup> D. Navarro,<sup>10</sup> G. Parisi,<sup>8,9</sup> S. Perez-Gaviro,<sup>11,4</sup> F. Ricci-Tersenghi,<sup>8,9</sup> J.J. Ruiz-Lorenzo,<sup>12,4</sup> S.F. Schifano,<sup>13</sup> B. Seoane,<sup>14,4</sup> A. Tarancon,<sup>3,4</sup> R. Tripiccionne,<sup>2</sup> and D. Yllanes<sup>15,4</sup>  
(Janus Collaboration)

<sup>1</sup>*Institut de Physique Théorique, DRF, CEA Saclay, F-91191 Gif-sur-Yvette Cedex, France*

<sup>2</sup>*Dipartimento di Fisica e Scienze della Terra, Università di Ferrara e INFN, Sezione di Ferrara, Ferrara, Italy*

<sup>3</sup>*Departamento de Física Teórica, Universidad de Zaragoza, 50009 Zaragoza, Spain*

<sup>4</sup>*Instituto de Biocomputación y Física de Sistemas Complejos (BIFI), 50009 Zaragoza, Spain*

<sup>5</sup>*Departamento de Física Teórica I, Universidad Complutense, 28040 Madrid, Spain*

<sup>6</sup>*Departamento de Ingeniería Eléctrica, Electrónica y Automática, U. de Extremadura, 10071, Cáceres, Spain*

<sup>7</sup>*Fundación ARAID, Diputación General de Aragón, Zaragoza, Spain*

<sup>8</sup>*Dipartimento di Fisica, Sapienza Università di Roma,*

*Istituto Nazionale di Fisica Nucleare, Sezione di Roma I, I-00185 Rome, Italy*

<sup>9</sup>*Istituto per i Processi Chimico-Fisici Consiglio Nazionale delle Ricerche, I-00185 Rome, Italy*

<sup>10</sup>*Departamento de Ingeniería, Electrónica y Comunicaciones and I3A, U. de Zaragoza, 50018 Zaragoza, Spain*

<sup>11</sup>*Centro Universitario de la Defensa, Carretera de Huesca s/n, 50090 Zaragoza, Spain*

<sup>12</sup>*Departamento de Física and Instituto de Computación Científica Avanzada (ICCAEx),  
Universidad de Extremadura, 06071 Badajoz, Spain*

<sup>13</sup>*Dipartimento di Matematica e Informatica, Università di Ferrara e INFN, Sezione di Ferrara, Ferrara, Italy*

<sup>14</sup>*Laboratoire de Physique Théorique, École Normale Supérieure & Université de Recherche Paris Sciences et Lettres,  
Pierre et Marie Curie & Sorbonne Universités, UMR 8549 CNRS, 75005 Paris, France*

<sup>15</sup>*Department of Physics and Soft Matter Program, Syracuse University, Syracuse, NY, 13244*

(Dated: October 6, 2016)

The unifying feature of glass formers (such as polymers, supercooled liquids, colloids, granulars, spin glasses, superconductors, ...) is a sluggish dynamics at low temperatures. Indeed, their dynamics is so slow that thermal equilibrium is never reached in macroscopic samples: in analogy with living beings, glasses are said to age. Here, we show how to relate experimentally relevant quantities with the experimentally unreachable low-temperature equilibrium phase. We have performed a very accurate computation of the non-equilibrium fluctuation-dissipation ratio for the three-dimensional Edwards-Anderson Ising spin glass, by means of large-scale simulations on the special-purpose computers Janus and Janus II. This ratio (computed for finite times on very large, effectively infinite, systems) is compared with the equilibrium probability distribution of the spin overlap for finite sizes. The resulting quantitative statics-dynamics dictionary, based on observables that can be measured with current experimental methods, could allow the experimental exploration of important features of the spin-glass phase without uncontrollable extrapolations to infinite times or system sizes.

Theory and Experiment follow apparently diverging paths when studying the glass transition. On the one hand, experimental glass formers (spin glasses, fragile molecular glasses, polymers, colloids, ...) undergo a dramatic increase of characteristic times when cooled down to their glass temperature,  $T_g$  [1]. Below  $T_g$ , the glass is always out of equilibrium and *aging* appears [2]. Consider a rapid quench from a high temperature to the working temperature  $T$  ( $T < T_g$ ), where the system is left to equilibrate for time  $t_w$  and probed at a later time  $t + t_w$ . Response functions such as the magnetic susceptibility turn out to depend on  $t/t_w^\mu$ , with  $\mu \approx 1$  [2–4]. The age of the glass,  $t_w$ , remains the relevant time scale even for  $t_w$  as large as several days. On the other hand, theoreticians find it easier to compute equilibrium properties (e.g., non-linear magnetic susceptibilities), either for finite or infinite systems. Relating this equilibrium information to the aging experimental responses is an open problem.

A promising way to fill the gap is to establish a statics-dynamics dictionary (SDD) [5–8]: non-equilibrium properties at *finite times*  $t$ ,  $t_w$ , as obtained on samples of macroscopic size  $L \rightarrow \infty$ , are quantitatively matched to equilibrium quantities computed on systems of *finite size*  $L$  [the SDD is an  $L \leftrightarrow (t, t_w)$  correspondence]. Clearly, in order for it to be of any value, an SDD cannot strongly depend on the particular pair of aging and equilibrium quantities that are matched.

Some time ago, we proposed one such a SDD [6–8]. However, this SDD was unsatisfactory in two respects. First,  $L$  was matched only to  $t_w$  (irrespectively of the probing time  $t + t_w$ ). Second, our SDD matched spatial correlation functions whose experimental study is only incipient [9, 10].

A different approach was advocated by Barrat and Berthier [5], who suggested building an SDD through the pattern of violations of the Fluctuation-Dissipation Theorem (FDT) [11–19]. However, the feasibility (for

glasses) of this approach is a non-trivial statement that needs to be established. Indeed, as we argue below the FDT-based SDD does *not* exist for ferromagnets.

Let us remark that FDT violations carry crucial information [11, 14, 15]: they provide a promising experimental path towards measuring Parisi's functional order parameter [20]. As a consequence the pattern of FDT violations has attracted much attention. One encounters numerical studies for both Ising [13, 16, 18] and Heisenberg [21, 22] spin glasses, as well as for structural glasses [23–27]. On the experimental side, we have studies on atomic spin glasses [17, 19], superspin glasses [10], polymers [9, 28], colloids [29–35] or DNA [36].

Here, we perform a detailed simulation of FDT violations in the three-dimensional Ising spin glass employing the custom-made supercomputers Janus [37] and Janus II [38]. In fact, this has been the launching simulation campaign of the Janus II machine, which was designed with this sort of dynamical studies in mind. Our simulations stand out by the spanned time range (11 orders of magnitude), by our high statistical accuracy and by the range of system sizes, enabling us to control size effects ( $L = 20, 40, 80$  and  $160$ ). Thus armed, we assess whether or not an SDD can be built from these violations, and compare the SDD proposed in this paper with other proposals. We focus on spin glasses, rather than on other model glasses, for a number of reasons: (i) their sluggish dynamics is known to be due to a thermodynamic phase transition at  $T_c = T_g$  [39–41]; (ii) the size of the *glassy* magnetic domains,  $\xi(t_w)$ , is experimentally accessible [42, 43] ( $\xi \sim 100$  lattice spacings [42], much larger than comparable measurements for structural glasses [44]); (iii) a restricted FDT-based SDD, see Eq. (4) below, has been well established [11, 14, 15]; (iv) FDT violations have been studied experimentally [17]; (v) well developed, yet mutually contrasting, theoretical scenarios are available for spin glasses in equilibrium [45]; (vi) magnetic systems are notably easier to model and to simulate numerically (in fact, special-purpose computers have been built for the simulation of spin glasses [37, 38, 46–48]).

*FDT violations and the SDD* — We suddenly cool a three-dimensional spin-glass sample of size  $L^3$  from high temperature to the working (sub-critical) temperature  $T = 0.7 = 0.64T_c$  at the initial time  $t_w = 0$  (see Appendix A, below, for more details and definitions). During the non-equilibrium relaxation a coherence length  $\xi(t_w)$  grows [6, 42, 49], which is representative of the size of the spin-glass domains. Then, from the waiting time  $t_w$  on, we place the system under a magnetic field of strength  $H$ , and consider the response function at a later measuring time  $t + t_w$

$$\chi_L(t + t_w, t_w) = \left. \frac{\partial m_L(t + t_w)}{\partial H} \right|_{H=0}, \quad (1)$$

where  $m_L(t + t_w)$  is the magnetization density in a sample of linear size  $L$ . This susceptibility is then compared with the spin temporal correlation function  $C_L(t + t_w, t_w)$ .

From now on, we shall take the limits

$$\chi(t + t_w, t_w) = \lim_{L \rightarrow \infty} \chi_L(t + t_w, t_w), \quad (2)$$

$$C(t + t_w, t_w) = \lim_{L \rightarrow \infty} C_L(t + t_w, t_w), \quad (3)$$

which are easy to control numerically: if  $L > 7\xi(t + t_w)$  size effects are negligible [6] (see also Appendix F).

The FDT states that  $T\chi(t + t_w, t_w) = 1 - C(t + t_w, t_w)$ , with both  $\chi$  and  $C$  computed at  $H = 0$ . However, for  $T < T_c$  the FDT does not hold. In fact, FDT violations take the form [11, 14, 15] (the order of limits is crucial):

$$\lim_{t_w \rightarrow \infty} T\chi(t + t_w, t_w) = \lim_{t_w \rightarrow \infty} \left[ \lim_{L \rightarrow \infty} S(C_L(t + t_w, t_w), L) \right], \quad (4)$$

where  $t$  is scaled as  $t_w$  grows, to ensure that the full range  $0 < C(t + t_w, t_w) < 1$  gets covered, and  $S(C, L)$  is given by a double integral of  $P(q, L)$ , the equilibrium distribution function of the spin overlap [see Eq. (A3)].

Here, we mimic an experimental protocol [17, 19] in that we consider the non-equilibrium response on a very large system but at *finite times*. We try to relate this response with the equilibrium overlap for a system of finite effective size  $L_{\text{eff}}$

$$T\chi(t + t_w, t_w) = S(C(t + t_w, t_w), L_{\text{eff}}(t + t_w, t_w)), \quad (5)$$

where we have assumed that both  $\chi$  and  $C$  have reached their thermodynamic limit. The same approach was followed for a two-dimensional spin glass by Barrat and Berthier [5] (note, however, that there is no stable spin-glass phase at  $T > 0$  in two spatial dimensions).

Eq. (5) provides a statics-dynamics dictionary (SDD) relating both times  $t$  and  $t_w$  with a single effective equilibrium size  $L_{\text{eff}}(t + t_w, t_w)$ . Note that it is not obvious a priori that our program can be carried out. For instance, our SDD does not exist for ferromagnets: one can readily show that  $S(C, L) \leq 1 - \langle |q| \rangle_{L=\infty}$ , see Appendix G, but  $T\chi(t + t_w, t_w)$  grows in ferromagnets well above this bound [50, 51].

SDDs based on the comparison of aging and equilibrium correlation functions (rather than on FDT violations) have been studied in some detail [7, 8, 52]. It was found that the effective length depends solely on  $t_w$ . Indeed,

$$L_{\text{eff}}(t + t_w, t_w) = k \xi(t_w), \quad (6)$$

with  $k \approx 3.7$ , was accurate enough to match the correlation functions [7, 8]. Ref. [5] also agreed with Eq. (6). In fact, Eq. (6) also underlies the analysis of Refs. [53, 54]. Yet, we shall show below that Eq. (6) is oversimplified.

*Numerical data* — The three basic quantities computed in this work, namely  $\chi(t + t_w, t_w)$ ,  $C(t + t_w, t_w)$  and  $\xi(t_w)$  are displayed in Fig. 1. Full details about this computation are provided in Appendix C.

Let us remark that the Janus II supercomputer allows us to probe unexplored dynamical regimes, either  $t/t_w$  as

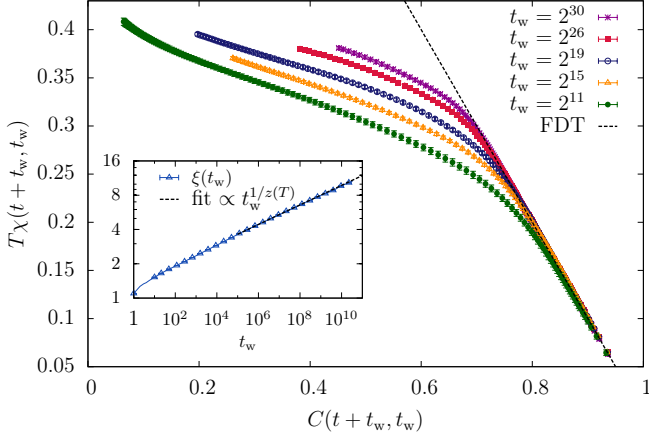


FIG. 1. Response function  $T\chi(t + t_w, t_w)$  versus  $C(t + t_w, t_w)$  at  $T = 0.7$  [for fixed  $t_w$ ,  $C(t + t_w, t_w)$  monotonically decreases from  $C = 1$  at  $t = 0$  to  $C = 0$  at  $t = \infty$ ]. Data for  $t_w = 2^{11}$  and  $t_w = 2^{30}$  was obtained on Janus II (the other  $t_w$  are from Janus). The five values of  $t_w$  correspond to effective equilibrium sizes  $L_{\text{eff}}$  that, according to Eq. (6), span the size range investigated in Ref. [7] (namely,  $8 \leq L \leq 32$ ). **Inset:** growth of the spin-glass coherence length  $\xi(t_w)$  as a function of time, computed at zero magnetic field and following Refs. [6, 49], from simulations of  $L = 160$  lattices at  $T = 0.7$  on Janus II. In dashed lines we plot the scaling  $\xi(t_w) \propto t_w^{1/z(T)}$  with  $z(T) = 11.64$  from Ref. [48].

large as  $1.4 \times 10^7$  (i.e., we follow the magnetic response for a very long time, after the field was switched on at  $t_w = 2^{11}$ ) or  $t_w$  as large as  $2^{30}$  (i.e., we study the response of a very old spin glass, but we are limited to  $t/t_w \approx 27$  in this case).

It is also remarkable that we are able to compute both the susceptibility  $\chi$  and the correlation function  $C$  without worrying about finite-size effects. Indeed, size effects become visible when the coherence length reaches the threshold  $\xi(t_w) = L/7$  [6] which in our  $L = 160$  lattice translates to  $\xi \approx 23$  lattice spacings. As Fig. 1-inset shows, we are quite far from this safety threshold.

With respect to previous measurements of the FDT ratio, it is worth stressing that now we are able to take the  $h \rightarrow 0$  limit in a more controlled way. This is far from trivial, given that the linear response regime shrinks to very small field when  $t_w$  increases (see Appendix C).

The data in Fig. 1 also stands out by its statistical accuracy (due to the large number of samples and large system sizes we simulated, but also thanks to the analysis method described in Appendix D. As a consequence, the violations to the FDT  $T\chi(t, t_w) = 1 - C(t, t_w)$  can be studied in great detail. In particular, the reader might be stricken by the linear behavior at  $C(t + t_w, t_w) \approx 0.4$ . In fact, following Refs. [11, 14, 15], this linear behavior could be interpreted as evidence for one step of replica-symmetry breaking (see, for instance, Ref. [55]). However, we shall argue below that the effective length in Eq. (5) evolves as time  $t$  grows, thus producing an up-

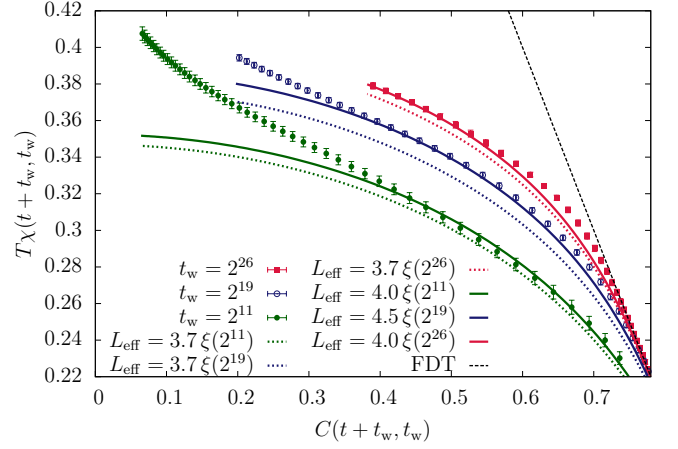


FIG. 2. Close-up of Fig. 1 (we only show data for three  $t_w$ , for the sake of clarity). Lines are  $S(C, L_{\text{eff}})$ , recall Eq. (5), with the effective equilibrium size as in Eq. (6):  $L_{\text{eff}}(t + t_w, t_w) = k\xi(t_w)$ . Dotted lines correspond to  $k = 3.7$ , which is the proportionality constant that was found by matching equilibrium and non-equilibrium correlation functions [6–8]. The continuous lines were found by choosing the best possible  $k$  for each  $t_w$ . This representation shows that the single-time static-dynamics dictionary  $L_{\text{eff}} \sim \xi(t_w)$  breaks down for large  $t$ , when  $\xi(t + t_w)$  is much larger than  $\xi(t_w)$ .

turn in the response which is probably responsible for the linear behavior in Fig. 1.

Let us make a final remark. We know that  $S(C, L)$  is upper bounded by  $1 - \overline{|q|}_{L=\infty} \geq 1 - q_{\text{EA}}^{(L=\infty)}$ . Now, at  $T = 0.7$  we know that  $1 - q_{\text{EA}}^{(L=\infty)} = 0.48(3)$  [8] (or  $0.46(3)$  [7]). Therefore, the dynamic responses  $T\chi(t, t_w)$  in Fig. 1 are well below  $1 - q_{\text{EA}}^{(L=\infty)}$ , at variance with ferromagnets [50, 51]. It follows that the effective length in Eq. (5) can be perfectly defined for three-dimensional spin glasses.

*The effective equilibrium size* — As we show in Fig. 2, our data are too accurate to be quantitatively described by combining Eq. (5) with Eq. (6). This simple description fails both at short times  $t$  (i.e., when  $C(t, t_w) \approx q_{\text{EA}}^{[L \approx 4\xi(t_w)]}$ ) and also at very long  $t$ , although one can find a constant  $k$  that works well for intermediate  $t$ .

The discrepancy for long  $t$  seems easy to rationalize: since the growth of  $\xi(t_w)$  is very slow, recall Fig. 1-inset,  $\xi(t + t_w)$  and  $\xi(t_w)$  are very similar to each other for small  $t$  and, therefore,  $L_{\text{eff}} \propto \xi(t_w)$  makes sense. However, since  $\xi(t_w)$  grows without bounds in the spin-glass phase, one should eventually have  $\xi(t + t_w) \gg \xi(t_w)$ . Under these circumstances, it is only natural that  $L_{\text{eff}} \propto \xi(t + t_w)$ .

We can test this proposal by computing an exact  $L_{\text{eff}}$  for each  $(t, t_w)$  pair (see Appendix E for details), which we plot in Fig. 3: in the main panel in units of  $\xi(t + t_w)$  and in the inset in units of  $\xi(t_w)$ .

The first important observation from the main panel in Fig. 3 is that, for long enough times, we find  $L_{\text{eff}} \approx$

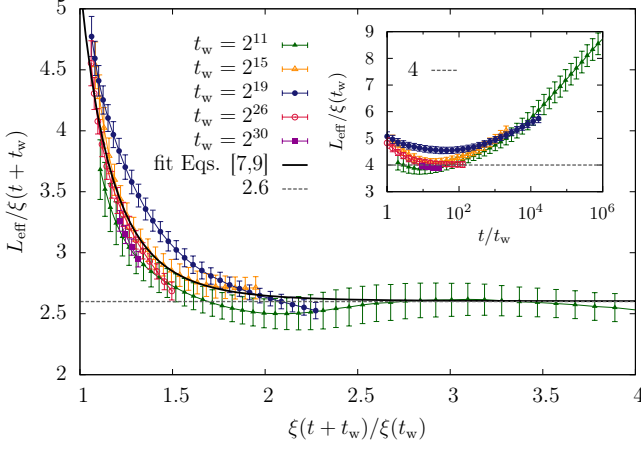


FIG. 3. For each  $t_w$ , we show the effective equilibrium side  $L_{\text{eff}}(t + t_w, t_w)$  in units of the coherence length at the measuring time  $\xi(t + t_w)/\xi(t_w)$  versus the ratio of coherence lengths  $\xi(t + t_w)/\xi(t_w)$  (recall that  $t$  is the time elapsed since switching-on the magnetic field). The ratio of coherence lengths is 1 for  $t = 0$  and goes as  $\xi(t + t_w)/\xi(t_w) \propto (1 + t/t_w)^{1/z(T)}$  for large time, with  $z(T = 0.7) = 11.64(15)$  [49]. Let us stress that there is no extrapolation in this figure, only interpolation (i.e.,  $L_{\text{eff}}$  falls within the simulated equilibrium sizes,  $8 \leq L_{\text{eff}} \leq 32$ ). The solid line is a fit to the scaling function  $h(x)$  in Eq. (7) and Eq. (9). **Inset:**  $L_{\text{eff}}(t + t_w, t_w)$  data from the main panel in units of the coherence length at the initial time  $\xi(t_w)$ , as a function of the time ratio  $t/t_w$ .

$2.6 \xi(t + t_w)$ , in agreement with the intuition exposed above. This is definitely different from Eq. (5), used until now. The data in the inset of Fig. 3 explain why the previous relation in Eq. (5) passed many numerical tests until now: the non-monotonic behavior of  $L_{\text{eff}}/\xi(t_w)$  for short times  $t$  makes this ratio roughly compatible with a constant  $k \approx 4$  as long as  $t/t_w \lesssim 1000$ .

Surprisingly, the ratio  $L_{\text{eff}}/\xi(t + t_w)$ , or equivalently  $L_{\text{eff}}/\xi(t_w)$ , becomes large as well when  $t \rightarrow 0$ , thus explaining the inability of Eq. (5) in describing dynamical data at short times  $t$  (see Fig. 2). Nonetheless in the limit  $t \rightarrow 0$ , i.e.  $\xi(t + t_w)/\xi(t_w) \rightarrow 1$ , the effective equilibrium size  $L_{\text{eff}}$  seems to reach a finite value; a divergence of  $L_{\text{eff}}$  in this limit seems unlikely (see Appendix H).

*$L_{\text{eff}}$  and the spin-glass coherence length* — Now that it is clear that both  $\xi(t_w)$  and  $\xi(t + t_w)$  are relevant for  $L_{\text{eff}}$  one may ask about the crossover between the  $\xi(t_w)$ -dominated regime and the  $\xi(t + t_w)$ -dominated regime. Fig. 3 tells us that  $L_{\text{eff}}/\xi(t + t_w)$  is, to a good approximation, a function of the ratio  $\xi(t + t_w)/\xi(t_w)$  [56]. Thus, we attempted to fit the crossover with the functional form

$$L_{\text{eff}}(t + t_w, t_w) = \xi(t + t_w) h(\xi(t + t_w)/\xi(t_w)), \quad (7)$$

where the scaling function is

$$h(x) = k_1 + k_2 x^{-c}. \quad (8)$$

Interpolation of data shown in Fig. 3 returns:  $k_1 = 2.58(2)$ ,  $k_2 = 2.7(1)$  and  $c = 5.9(2)$ . Noticing that

$k_2 \approx k_1$  and  $c \approx z(T)/2$ , where  $z(T)$  is the exponent for the time growth of the coherence length,  $z(T = 0.7) = 11.64(15)$  (see Fig. 1-inset, and Refs. [6, 49]), the scaling function  $h(x)$  can be also rewritten in a much simpler form as

$$h(\xi(t + t_w)/\xi(t_w)) = k_1 \left( 1 + \sqrt{\frac{t_w}{t + t_w}} \right) \quad (9)$$

Fitting data in Fig. 3 with this simpler scaling function returns  $k_1 = 2.59(1)$  (see full curve in Fig. 3). Given that the fit with 3 adjustable parameters in Eq. (8) and the one in Eq. (9) with just 1 adjustable parameter have practically the same quality-of-fit, we tend to prefer the simpler ansatz, as long as it interpolates the numerical data well enough.

The ultimate check for the success of Eq. (7) and Eq. (9) in reproducing the aging response is provided by Fig. 4, where the dynamical measurements (data points with errors) are plotted together with the equilibrium function  $S(C(t + t_w, t_w), L_{\text{eff}}(t + t_w, t_w))$ . The very good agreement in the whole range gives a strong support in favor of an SDD based on Eq. (7) and Eq. (9).

Note as well that Eq. (7) explains the previous success of the simpler SDD in Eq. (6). In fact, at short times  $t$ , the two coherence lengths  $\xi(t + t_w)$  and  $\xi(t_w)$  are very similar to each other, and the amplitude  $k$  in Eq. (6) is essentially  $k = k_1 + k_2 \approx 2k_1$ .

The ansatz of Eq. (7) provides as well a simple explanation for the upturn of the aging response at small values of  $C$ , recall Fig. 1. Indeed, as time  $t$  increases, the correlation function decays as  $C \propto (t + t_w)^{-1/\alpha}$ ,  $\alpha \approx 7$  [6]. But, from  $\xi(t + t_w) \propto (t + t_w)^{1/z(T)}$  we conclude that, even at fixed  $t_w$ ,  $L_{\text{eff}}$  diverges for large  $t$  as  $C^{-7/z(T)}$ . Now, to a first approximation, one may expect that  $S(C, L = \infty) - S(C, L) \propto L^{-\theta \approx -0.38}$  (see the description of the overlap distribution function in Appendix A). We thus expect the susceptibility to approach its  $C = 0$  limit in a singular way, as  $C^{\theta/(\alpha z(T))} \approx C^{0.23}$ .

*Which features of the  $P(q)$  can be obtained from dynamic measurements?* — One of the major gains of the present analysis would be to obtain Parisi's functional order parameter  $P(q)$  from experimental dynamic data. In an ideal situation, one would have data for  $\chi$ ,  $C$  and  $\xi$ , complemented by the ansatz in Eq. (9). Then, one would like to know which features of the underlying  $S(C, L)$  can be retrieved from these dynamic measurements.

In order to answer this question, we have considered a very simplified  $P_{\text{simpl}}(q, L)$ , that possesses the main features of the  $P(q, L)$  measured in numerical simulations (see Appendix A):

$$P_{\text{simpl}}(q, L) = (P_0 + P_1 q^2) \theta(q_{\text{EA}}^{(L)} - q) + w^{(L)} \delta(q - q_{\text{EA}}^{(L)}), \quad (10)$$

where  $P_0$  and  $P_1$  are constants,  $\theta(x)$  is the Heaviside step function and  $w^{(L)}$  is a weight enforcing normaliza-

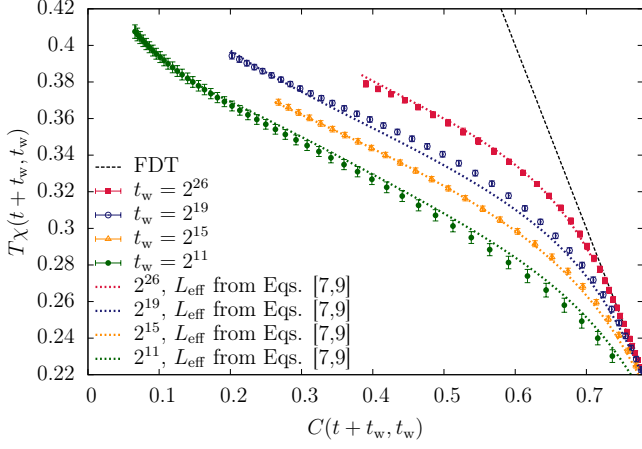


FIG. 4. As in Fig. 2 but  $L_{\text{eff}}$  is taken from the ansatz in Eq. (7) and Eq. (9), which improves on the single-time statics-dynamics dictionary based on  $\xi(t_w)$  by considering a crossover to a  $\xi(t + t_w)$ -dominated regime.

tion [57]. Integrating  $P_{\text{simpl}}(q, L)$  twice we get

$$S_{\text{simpl}}(C, L) = \min \left[ S_0(L) - P_0 C^2 - \frac{P_1}{6} C^4, 1 - C \right]. \quad (11)$$

$S_0(L) = S(0, L)$  is taken from the true  $P(q, L)$ . Recall that  $S(0, L) = 1 - \overline{\langle q \rangle}_L$ , Eq. (G5). Instead, the  $L$ -independent  $P_0$  and  $P_1$  are fitted in order to obtain a  $S_{\text{simpl}}(C, L)$  as similar as possible to the true  $S(C, L)$ . In other words,  $P_{\text{simpl}}(q)$  shares with the true distribution only four numeric features: normalization, first moment  $\overline{\langle q \rangle}_L$ ,  $P_0 \simeq P(q = 0, L)$  which is essentially  $L$ -independent, and the second derivative  $P_1 \simeq P''(q = 0, L)/2$ . In particular, note that having  $P_0 > 0$  is a crucial feature of the mean-field solution [58].

The outcome of this analysis is given in Fig. 5. It turns out that the simplified  $S_{\text{simpl}}$  in Eq. (11), is almost as effective as the true  $S(C, L)$  in representing the non-equilibrium data through the effective size  $L_{\text{eff}}$  in Eq. (9). The only obvious disagreement is that Eq. (11) predicts a non-analytic behavior for the susceptibility  $\chi$  at  $C = q_{\text{EA}}^{L_{\text{eff}}}$ , which is not found in our non-equilibrium data. In other words, the effective size for times such that  $C(t + t_w, t_w) \sim q_{\text{EA}}^{[L \approx 4\xi(t_w)]}$  is large, but certainly  $L_{\text{eff}}$  is not infinite as demanded by Eq. (10).

Fortunately, even the crude description in Eq. (11) could lead to some interesting analysis. For instance, one could select pair of times  $(t, t_w)$  such that  $L_{\text{eff}}(t + t_w, t_w) = \text{constant}$ . Then,  $S(0, L_{\text{eff}})$  will be the same for all those points. Now, we note from Eq. (9) that  $\xi(t + t_w)$  can vary by as much as a factor of two, for such points. It follows that  $C(t + t_w, t_w)$  should vary significantly over this set of times with fixed  $L_{\text{eff}}(t + t_w, t_w)$ . Hence, the crucial parameters  $P_0$  and  $P_1$  could be extracted. For instance, if the susceptibility  $\chi(t + t_w, t_w)$  would turn out not to depend on  $C(t + t_w, t_w)$  (while keeping  $L_{\text{eff}}$  fixed), this would mean  $P_0, P_1 \approx 0$ , in contrast with the mean

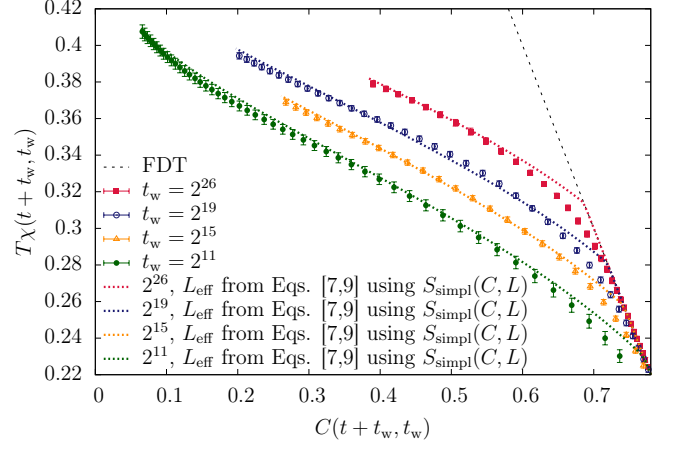


FIG. 5. As in Fig. 4 but this time we use the simplified  $S_{\text{simpl}}(C, L)$  from Eq. (11). Note that dynamic data are well reproduced by Eq. (7) and Eq. (9), even in this simple approximation.

field prediction  $P_0 > 0$ .

*Discussion* — It was discovered some twenty years ago that experimental aging response functions carry information on Parisi's functional order parameter [11–13]. We now know that this connection between non-equilibrium and equilibrium physics relies on a very general mathematical property, stochastic stability [14, 15], shared by many glass models. However, experimental attempts to explore this connection encountered a major problem [17, 19]: an essentially uncontrolled extrapolation to infinite waiting time  $t_w$  is required.

Here, we have proposed employing a statics-dynamics dictionary [5–8] to avoid uncontrolled extrapolations. Indeed, we have shown that the aging responses at finite  $t_w$  can be connected to the Parisi's order parameter as computed at equilibrium in a system of finite size.

We have shown that this FDT-based SDD is essentially consistent with previous proposals [6–8] that focused on spatial correlation functions. This is an important consistency test. There is a caveat, though: when the probing time  $t + t_w$  is such that one has  $\xi(t + t_w) \gg \xi(t_w)$  for the coherence lengths, the FDT-based SDD disagrees from previous dictionaries in that the size of the equivalent equilibrium system is  $L_{\text{eff}} \sim \xi(t + t_w)$  (rather than  $L_{\text{eff}} \sim \xi(t_w)$ ). In fact, we have found that the  $L_{\text{eff}}$  dependence on both length scales can be simply parameterized, recall Eq. (7) and Eq. (9).

On the other hand, the only previous SDD known to us that was based on Eq. (5) misses the  $L_{\text{eff}} \sim \xi(t + t_w)$  behavior [5]. There are a couple of possible reasons for this failure. For one, the time scales in Ref. [5] do not allow for length-scale separation  $\xi(t + t_w) \gg \xi(t_w)$ . Besides, the SDD from Ref. [5] was obtained for two-dimensional spin glasses (which only have a paramagnetic phase). Therefore, the results of Ref. [5] are probably a manifestation of finite-time/finite-size scaling [52, 59].

Let us conclude by stressing that the three basic quan-

tities analyzed in this work, namely the susceptibility  $\chi(t + t_w, t_w)$ , the correlation function  $C(t + t_w, t_w)$  and the coherence length  $\xi(t + t_w)$ , have been obtained experimentally in a dynamic setting very similar to simulations (for  $\chi$  and  $C$ , see Refs. [17, 19], for  $\xi$  see Refs. [42, 43]). We thus think that it should be possible to extract the spin-glass functional order parameter from already existing experimental data. Furthermore, FDT violations have been studied as well in superspin glasses [10] and in a variety of soft condensed-matter systems [9, 28–36]. We therefore expect that our analysis will be of interest beyond the realm of spin glasses.

*Acknowledgments* — Some of the simulations in this work (the  $L < 80$  systems, to check for size effects) were carried out on the *Memento* cluster: we thank staff from BIFI’s supercomputing center for their assistance. We thank Giancarlo Ruocco for guidance on the experimental literature. We warmly thank M. Pivanti for his contribution to the early stages of the development of the

Janus II computer. We also thank Link Engineering (Bologna, Italy) for their precious role in the technical aspects related to the construction of Janus II. We thank EU, Government of Spain and Government of Aragon for the financial support (FEDER) of Janus II development. This work was partially supported by MINECO (Spain) through Grant Nos. FIS2012-35719-C02, FIS2013-42840-P, FIS2015-65078-C2, and by the Junta de Extremadura (Spain) through Grant No. GRU10158 (partially funded by FEDER). This project has received funding from the European Union’s Horizon 2020 research and innovation program under the Marie Skłodowska-Curie grant agreement No. 654971. This project has received funding from the European Research Council (ERC) under the European Union’s Horizon 2020 research and innovation program (grant agreement No 694925). DY acknowledges support by NSF-DMR-305184 and by the Soft Matter Program at Syracuse University. MBJ acknowledges the financial support from ERC grant NPRGGLASS.



## APPENDICES

A. Model and observables	7
B. Our simulations	7
C. Computation of the linear susceptibility	8
D. Smoothing and interpolating the data	8
E. Fit of $\mathcal{S}(C, L)$ and computation of $L_{\text{eff}}$	10
F. Finite-size effects in the response	10
G. A simple inequality	10
H. Extrapolating the effective size	11
I. The simplified $\mathcal{S}(C, L)$	12
References	12

### Appendix A: Model and observables

We study the  $D=3$  Edwards-Anderson model, whose Hamiltonian is given by

$$\mathcal{H} = - \sum_{\langle \mathbf{x}, \mathbf{y} \rangle} J_{\mathbf{x}, \mathbf{y}} \sigma_{\mathbf{x}} \sigma_{\mathbf{y}} - H \sum_{\mathbf{x}} \sigma_{\mathbf{x}}. \quad (\text{A1})$$

The spins  $s_{\mathbf{x}} = \pm 1$  are placed on the nodes,  $\mathbf{x}$ , of a cubic lattice of linear size  $L$  and we set periodic boundary conditions. The couplings  $J_{\mathbf{x}, \mathbf{y}} = \pm 1$ , which join nearest neighbors only, are chosen randomly with 50% probability and are quenched variables. For each choice of the couplings (one “sample”), we simulate two independent copies of the system,  $\{s_{\mathbf{x}}^{(1)}\}$  and  $\{s_{\mathbf{x}}^{(2)}\}$ . We denote by  $\langle \dots \rangle$  the average over the thermal noise and by  $\overline{(\dots)}$  the *subsequent* average over the samples. The model described by Eq. (A1) undergoes a SG transition at  $H = 0$  and  $T_c = 1.102(3)$  [60].

For our dynamical data we have run new non-equilibrium simulations on Memento, Janus and Janus II. We use heat-bath dynamics, in which one Monte Carlo step roughly corresponds to one picosecond of the experimental system [61]. See Appendix B for technical details of these simulations. The two main dynamical observables are the magnetization density  $m_L(t + t_w) = \overline{\sum_{\mathbf{x}} \langle s_{\mathbf{x}}(t + t_w) \rangle} / V$  and the spin temporal correlation function  $C_L(t + t_w, t_w; H) = \overline{\sum_{\mathbf{x}} \langle s_{\mathbf{x}}(t_w) s_{\mathbf{x}}(t + t_w) \rangle} / V$ .

Equilibrium results at  $T = 0.7$  are available for  $L \leq 8 \leq 32$  [7]. In this case the main quantity is the probability density function  $P(q, L)$  of the spin overlap  $q$ :

$$q \equiv \frac{1}{V} \sum_{\mathbf{x}} s_{\mathbf{x}}^{(1)} s_{\mathbf{x}}^{(2)}, \quad \overline{\langle q^k \rangle}_L = \int_{-1}^1 dq' (q')^k P(q', L). \quad (\text{A2})$$

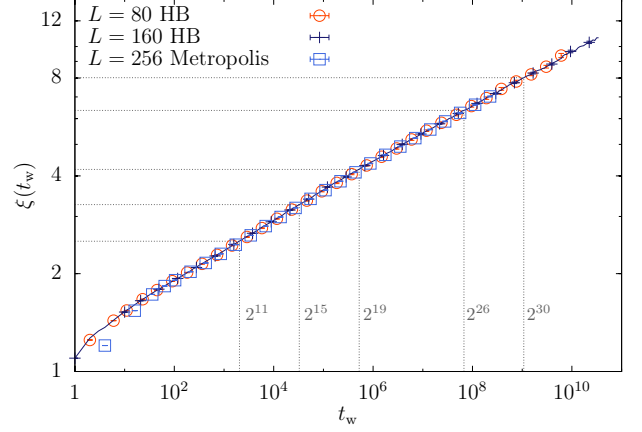


FIG. 6. Coherence length  $\xi(t_w)$  versus waiting time  $t_w$  at  $T = 0.7$  for different lattice sizes:  $L = 80$  (data taken from [49]),  $L = 160$  (new simulations) and  $L = 256$  (Metropolis dynamics from [52], rescaling the  $x$  axis by a factor of 4 to compare with our heat-bath dynamics). The dashed lines aim to point out the different  $t_w$  (and their corresponding  $\xi$ ) considered in this work.

In particular, we are interested in the integral

$$\begin{aligned} S(C, L) &= \int_C^1 dC' x(C', L), \\ x(C, L) &= \int_0^C dq 2P(q, L). \end{aligned} \quad (\text{A3})$$

The  $P(q, L)$  curves are easily described for finite  $L$ . They are symmetric under  $q \leftrightarrow -q$ , with two maxima at  $\pm q_{\text{EA}}^{(L)}$  and a flat central region. In the thermodynamic limit, the two peaks turn into delta functions at  $\pm q_{\text{EA}}^{(\infty)}$ , which mark the maximum possible value of  $|q|$ . The size evolutions, as checked for  $L \leq 32$  [7], are as follows:  $q_{\text{EA}}^{(L)} - q_{\text{EA}}^{(\infty)} \propto L^{-\theta \approx 0.38}$  (at  $T = 0.7$ ,  $q_{\text{EA}}^{(\infty)} = 0.52(3)$  [8]), the width of the peaks at  $\pm q_{\text{EA}}^{(L)}$  scales as  $L^{-B \approx 0.28}$  while  $P(q = 0, L)$  turns out to be greater than zero and  $L$ -independent.

### Appendix B: Our simulations

Using heat-bath dynamics on the Janus, Janus II and Memento supercomputers, we consider the following numerical experiment. Starting from a completely random configuration of the spins at  $T = 0.7$ , we first let the system evolve in absence of a magnetic field, i.e.  $H = 0$ , for a waiting time  $t_w$ . As this  $t_w$  grows, the spins rearrange in amorphous magnetic domains of increasing average size  $\xi$ , as we show in Fig. 6 ( $\xi$  is computed with the  $\xi_{12}$  integral estimator described in Refs. [6, 49]). After this time  $t_w$ , we turn on a tiny field  $H > 0$  and follow the response at a later time  $t + t_w$ .

We have considered five different values of  $t_w$ :  $t_w = 2^{11}$  and  $t_w = 2^{30}$  were simulated on Janus II;  $t_w = 2^{26}, 2^{19}$

and  $2^{15}$  on Janus (smaller systems were simulated on Memento, see below our study of size effects). Times are measured in units of Monte Carlo sweeps. The measuring times  $t$  were chosen as the integer part of  $2^{i/4}$  for integer  $i$  (discarding repetitions). For each  $t_w$  we repeat the procedure described above for four values of the magnetic field:  $H \in \{0, 0.02, 0.04, 0.08\}$  in the case of Memento and Janus I supercomputers and  $H \in \{0, 0.01, 0.02, 0.04\}$  on Janus II. We considered exactly the same set of samples with each  $H$  and reused the same sequences of random numbers in an effort to eliminate sources of fluctuations.

Depending on the computer used, we simulated different system sizes, either  $L = 80$  (on Memento and Janus I) or  $L = 160$  (on Janus II). We simulated 647 samples for  $L = 80$  (all  $t_w$  and  $H$  values). For  $L = 160$ , we used 55 samples for  $t_w = 2^{11}$  and 335 samples for  $t_w = 2^{30}$  [we also simulated 336 samples at  $H = 0$  in order to compute  $\xi(t_w)$ ]. Notice that self-averaging means that one needs fewer samples for larger sizes. Previous works at  $H = 0$  suggested that finite-size effects should be negligible, compared to our typical statistical accuracy, as long as we ensure that  $L > 7\xi(t + t_w)$  [6]. As a new test of the validity of this statement, we compare our new results of  $\xi(t_w)$  obtained with Janus II and  $L = 160$  with previous works corresponding to  $L = 80$  [49] and  $L = 256$  [52] (see Fig. 6) finding no significant dependence on  $L$  in the studied range of  $t_w$ .

### Appendix C: Computation of the linear susceptibility

The discussion on the violations of FDT requires the computation of the linear susceptibility, that is, of

$$\chi(t + t_w, t_w) = \left. \frac{\partial m(t + t_w)}{\partial H} \right|_{H=0}. \quad (C1)$$

With this aim, we measure  $m(t, t_w)/H$  at several values of the external field, and use them to extract the  $H \rightarrow 0$  limit. Indeed, since the Edwards-Anderson Hamiltonian is odd in the field around  $H = 0$ , one can write the magnetization in terms of odd powers of  $H$ , which allows us to separate the linear response  $\chi$  from the non-linear responses

$$m(t + t_w, t_w; H) = H\chi(t + t_w, t_w) - \frac{H^3}{3!}\chi_{NL}(t + t_w, t_w; H). \quad (C2)$$

In order to make some progress, we Taylor-expand  $\chi_{NL} = \chi_3 + \frac{H^2}{20}\chi_5 + \mathcal{O}(H^4)$ , thus finding:

$$\begin{aligned} \frac{m(t + t_w, t_w)}{H} &= \chi(t + t_w, t_w) - \frac{H^2}{3!}\chi_3(t + t_w, t_w) \\ &\quad - \frac{H^4}{5!}\chi_5(t + t_w, t_w) + \mathcal{O}(H^6), \end{aligned} \quad (C3)$$

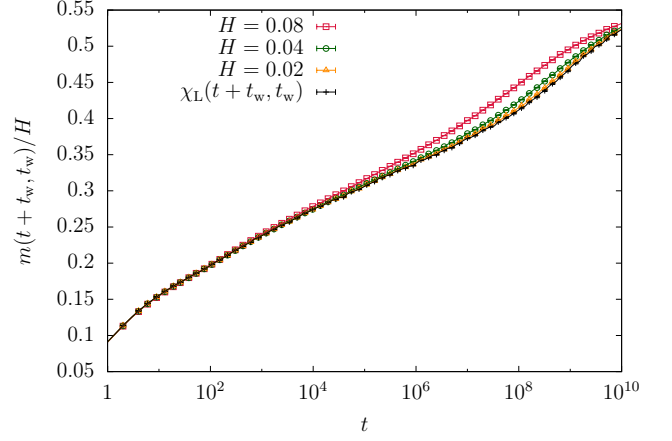


FIG. 7. Extraction of the linear susceptibility as a function of  $t$  from the  $m(t + t_w, t_w)/H$  data obtained at  $H = 0.02, 0.04$  and  $0.08$ . Data shown here corresponds to  $t_w = 2^{26}$ . For the sake of visibility, only one every two measured times have been plotted in points.

Therefore, if we measure  $m$  for three small fields and neglect higher-order contributions in  $H$ , we can extract  $\chi(t + t_w, t_w)$  from a set of three equations and three unknowns [by the same token, we obtain  $\chi_3(t + t_w, t_w)$  and  $\chi_5(t + t_w, t_w)$  as well, but these magnitudes will not be discussed herein]. We show in Fig. 7  $m(t + t_w, t_w)/H$  and  $\chi(t + t_w, t_w)$  for one of our values of  $t_w$ .

Alternatively, instead of performing simulations at different  $H$ , one could have obtained  $\chi(t + t_w, t_w)$  directly from simulations at  $H = 0$  using methods such as those described in Refs. [51, 62]. The drawback of this approach is that it would have required a much larger amount of samples in order to get equivalent statistical errors.

### Appendix D: Smoothing and interpolating the data

The original data consisted of pairs  $\{C(t + t_w, t_w), \chi(t + t_w, t_w)\}$ , where  $t$  takes some discrete values. However, if we reproduce Fig. 1 in the main text but using the raw measurements (see Fig. 8) we find much noisier curves. Indeed, data for successive times, although very correlated, displays random fluctuations. Besides, the statistical errors for  $C(t + t_w, t_w; H = 0)$  and  $C(t + t_w, t_w; H)$  are completely negligible compared to the errors in  $Tm(t + t_w, t_w; H)/H$  (they are indistinguishable in the figure). We used these two facts to our benefit in order to smooth and reduce the statistical errors of these curves. Let us describe our smoothing procedure step by step.

We fit our data for  $Tm(t + t_w, t_w; H)/H$  to a smooth function of

$$\hat{x}(t + t_w, t_w) = \frac{C(t + t_w, t_w) + C(t + t_w, t_w; H)}{2}. \quad (D1)$$



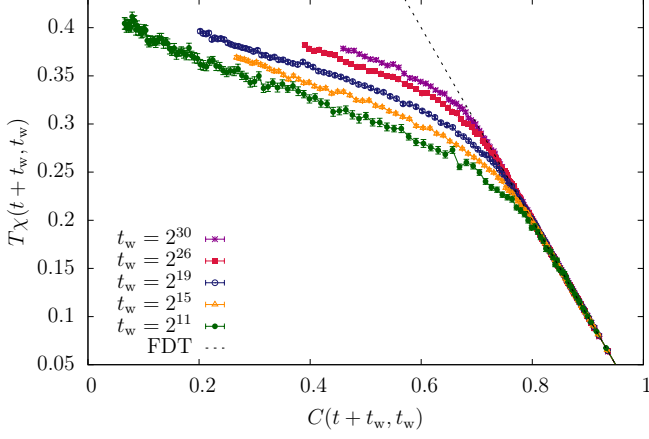


FIG. 8. Linear response  $T\chi(t, t_w)$  versus  $C(t + t_w, t_w)$  at  $T = 0.7$  and five values of  $t_w$  using raw processed data (to be compared with Fig. 1 in the main text, which was obtained only after the smoothing of the simulation data at fixed  $H$  and an extrapolation to  $H \rightarrow 0$ ).

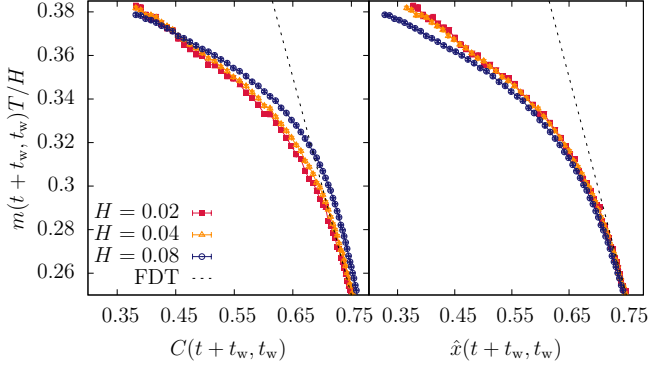


FIG. 9. Non-linear corrections in  $H$  to  $T\chi(t + t_w, t_w)$  when plotted versus  $C(t + t_w, t_w)$  (left) or  $x(t + t_w, t_w) = C(t + t_w, t_w) + C(t + t_w, t_w; H)/2$  (right). Data corresponds to  $t_w = 2^{26}$  and  $T = 0.7$ .

This choice [instead of just  $C(t + t_w, t_w)$ ], although irrelevant in the  $H \rightarrow 0$  limit, turns out to reduce the non-linear corrections in  $H$  as we show in Fig. 9, and yields easier and more accurate fits.

Our chosen functional form is as follows. Let the quantity  $Tm(t + t_w, t_w; H)/H$  be approximated by  $f(\hat{x})$  ( $f$  depends on  $H$  and  $t_w$ , but we will write  $f$  nevertheless, to keep the notation as light as possible):

$$f(\hat{x}) = f_L(\hat{x}) \frac{1 + \tanh[Q(\hat{x})]}{2} + f_S(\hat{x}) \frac{1 - \tanh[Q(\hat{x})]}{2}, \quad (D2)$$

with  $Q(\hat{x}) = (\hat{x} - \hat{x}^*)/w$ . In other words, there are two functional forms:  $f_S$ , adequate for small  $\hat{x}$  and  $f_L$ , good for large  $\hat{x}$ . The crossover between the two functional forms takes place at  $\hat{x}^* \approx 0.7$  in an interval of half-width

TABLE I. Information about the fits to Eqs. (D2,D3,D4).

$t_w$	$H$	$N$	$N'$	$\chi^2/\text{DOF}$
$2^{11}$	0.01	2	1	51.6822/127
	0.02	2	1	43.9926/127
	0.04	2	1	45.6321/127
$2^{15}$	0.02	2	1	33.1259/90
	0.04	2	1	43.3823/90
	0.08	2	2	21.0832/89
$2^{19}$	0.02	3	2	27.6364/115
	0.04	3	2	25.8737/115
	0.08	3	3	31.6819/114
$2^{26}$	0.02	2	1	29.5259/118
	0.04	2	1	36.5544/118
	0.08	2	1	57.3693/118
$2^{30}$	0.01	2	1	31.7369/126
	0.02	3	3	24.7701/122
	0.04	3	2	33.0019/123

$w \approx 0.04$  (although we keep  $\hat{x}^*$  and  $w$  as fitting parameters). The functional form for small  $\hat{x}$  are diagonal  $[N, N]$  Padé approximants,

$$f_S(\hat{x}) = \frac{\sum_{k=0}^N b_k \hat{x}^k}{\sum_{k=0}^N a_k \hat{x}^k}. \quad (D3)$$

As for the region where violations of the fluctuation-dissipation theorem are tiny, we chose a polynomial in  $1 - \hat{x}$

$$f_L(\hat{x}) = (1 - \hat{x}) + \sum_{k=2}^{N'} c_k (1 - \hat{x})^k. \quad (D4)$$

We keep  $a_k, b_k, c_k$  as fitting variables.

Following Refs. [6, 49, 52, 59], we perform a fit considering only the diagonal part of the covariance matrix (we obtain  $\chi^2/\text{DOF}$  significantly smaller than one, probably due to data correlation). Errors are computed following a jackknife procedure [we perform an independent fit for each jackknife block, and compute errors from the jackknife fluctuations of the fitted  $f(\hat{x})$ ]. Our fits are reported in Table I.

Once each curve  $Tm(t + t_w, t_w)/H$  is smoothed at each  $H$ , we extract the linear susceptibility following the procedure described in the previous Section. We show a comparison between the original and smoothed data in Fig. 10. We found that in most the cases the extrapolated linear response  $T\chi(t + t_w, t_w)$  was compatible within the error with the smaller field considered. However, the extrapolation  $H \rightarrow 0$  becomes particularly delicate and even changes the shape of the curve at large values of the  $t/t_w$  ratio, as we show in Fig. 11.

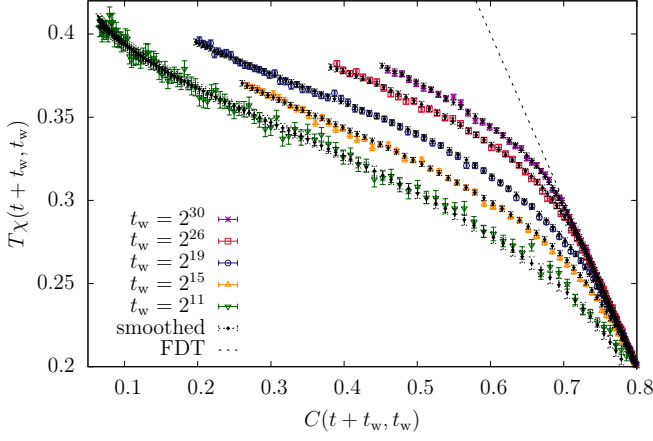


FIG. 10. Comparison between the original (in color and empty dots) and smoothed data (in black full dots) in the Linear response  $T\chi(t + t_w, t_w)$  versus  $C(t + t_w, t_w)$  curves. Data corresponds to  $T = 0.7$  and five values of  $t_w$ .

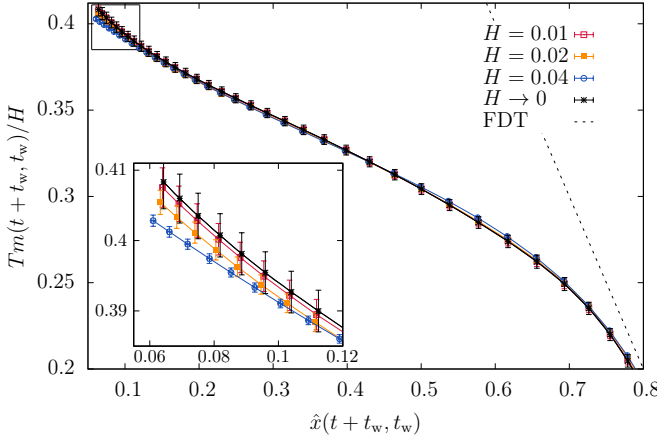


FIG. 11.  $Tm(t + t_w, t_w)/H$  versus  $\hat{x}(t + t_w, t_w)$  for several values of  $H$  (in color empty dots) and  $t_w = 2^{11}$ , together with the extrapolation  $H \rightarrow 0$  (in black crosses). The inset is a blow up of the region for large  $t/t_w$  in the square box.

#### Appendix E: Fit of $S(C, L)$ and computation of $L_{\text{eff}}$

Part of our discussion in the main text seeks to find a relation between the linear response at finite  $t_w$  with the overlap distribution  $P(q, L)$  in equilibrium at a finite size  $L_{\text{eff}}$ . That is,

$$T\chi(t + t_w, t_w) = S(C(t + t_w, t_w), L_{\text{eff}}(t + t_w, t_w)). \quad (\text{E1})$$

We computed  $S(C, L)$  by means of a numerical integration of the  $P(q, L)$  discussed in Ref. [7] for  $L = 8, 12, 16, 24$  and  $32$ . We show  $S(C, L)$  in the main panel of Fig. 12. In order to identify  $L_{\text{eff}}$  we needed a function  $S(q, x)$  that is continuous both in  $C$  and in  $L$ , which we construct by computing a cubic spline [63] of the data along both variables (first in  $C$  and only then in  $L$ ). Er-

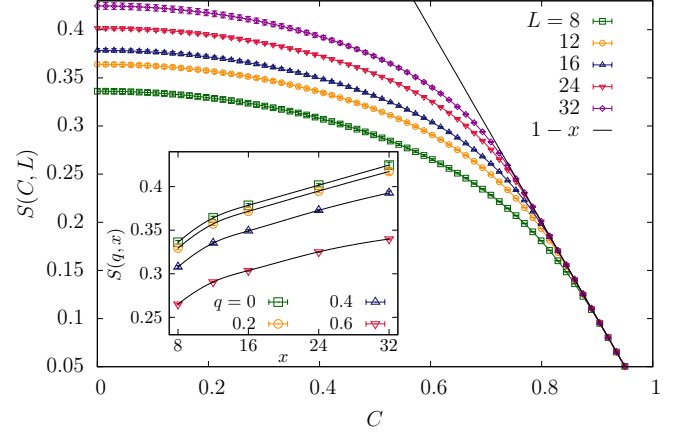


FIG. 12.  $S(C, L)$  versus  $C$  for different system sizes obtained using Eq. (A3) and data from Ref. [7]. (Inset) Orthogonal cuts to the figure in the main panel plotted as function of  $L$  in color points together with the interpolating cubic spline curve along this variable.

rors are computed using the jackknife method. We show some interpolation curves along the  $x$  variable in the inset of Fig. 12. Once  $S(q, x)$  is at hand,  $L_{\text{eff}}(t + t_w, t_w)$  can be extracted by looking for the  $x$  value that satisfies the Eq. (E1) at each time  $t$ , fixing the off-equilibrium data  $T\chi(t + t_w, t_w)$  and  $C(t, t_w)$ .

#### Appendix F: Finite-size effects in the response

Up to now, finite-size effects have been investigated only for single-time correlation functions [and the related extraction of  $\xi(t_w)$ ]. As far as we know, size effects were not studied previously in the response to a magnetic field  $\chi(t + t_w, t_w)$ . In this context, it is somewhat worrying that we have identified a large length scale  $L_{\text{eff}} \approx 100$  (discussed below) in the regime where violations of the FDT are incipient. For this reason, we have explicitly checked that our data does not suffer from finite-size effects in that region (as we show in Fig. 13) by comparing results from three system sizes,  $L = 20, 40$  and  $80$ , in the case of  $t_w = 2^{15}$ , finding no finite-size dependence. For the smaller system sizes we considered 28000 samples for  $L = 20$  and 12000 samples for  $L = 40$ .

#### Appendix G: A simple inequality

In the main text, we have used several times the inequality

$$S(C, L) \leq 1 - \overline{\langle |q| \rangle}_{L=\infty}. \quad (\text{G1})$$

Our purpose here is to remind the reader of its derivation, for the sake of completeness.

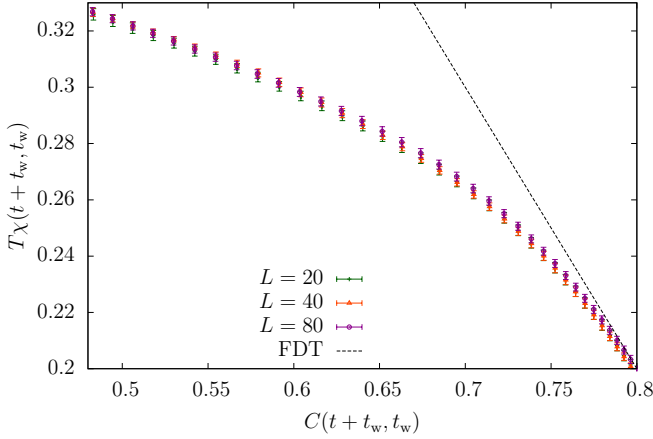


FIG. 13. Absence of finite-size effects in the response function  $T\chi(t + t_w, t_w)$  versus  $C(t + t_w, t_w)$  at  $T = 0.7$ . Data from  $L = 20, 40$  and  $80$  are compared in the case of  $t_w = 2^{15}$ . All the points are compatible within the error bars.

Let us first recall the notations used in the main text:

$$S(C, L) = \int_C^1 dC' x(C', L), \quad (\text{G2})$$

$$x(C, L) = \int_0^C dq 2P(q, L). \quad (\text{G3})$$

We start by noticing

$$S(C, L) \leq S(C = 0, L), \quad (\text{G4})$$

due to the inequality  $x(C, L) \geq 0$  for the cumulative distribution. Next, we integrate by parts to find [recall that  $P(q, L) = P(-q, L)$ ]

$$S(C = 0, L) = 1 - \overline{\langle |q| \rangle}_L, \quad \overline{\langle |q| \rangle}_L \equiv \int_{-1}^1 dq |q| P(q, L). \quad (\text{G5})$$

Finally, to obtain the upper bound in (G1), we remark that  $\overline{\langle |q| \rangle}_L$  is monotonically decreasing in  $L$  for a system with periodic boundary conditions.

## Appendix H: Extrapolating the effective size

We have shown in the main text that, for every  $t_w$  and small enough  $t$ ,  $L_{\text{eff}}(t + t_w, t_w)$  can be very large. This *short-time but large-size* effect arises when  $C(t + t_w, t_w) \approx q_{\text{EA}}^{L=4\xi(t_w)}$ . In fact, for  $t_w = 2^{30}$  (our largest) we can compute  $L_{\text{eff}}$  without extrapolations only for the largest  $t$ .

The above observation begs the question: how large can  $L_{\text{eff}}$  be in this small- $t$  regime? We provide here a crude extrapolation for our  $t_w = 2^{30}$  data, mostly based on the scaling laws found in [7].

We start by noticing that one could be tempted to extract the spin-overlap probability directly from the aging

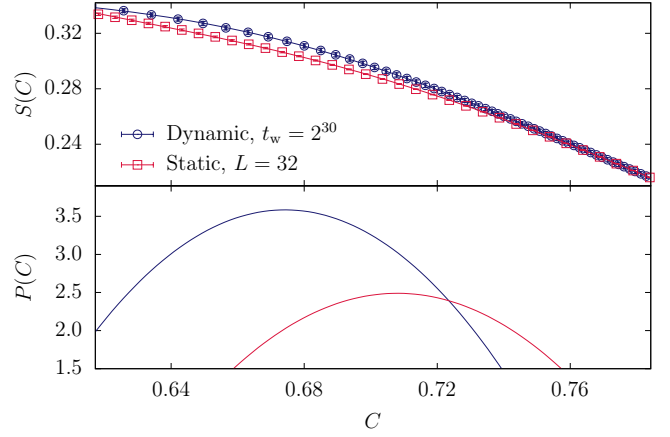


FIG. 14. Numerical attempt to locate the maximum of  $P_{\text{dyn}}(q, t_w = 2^{30})$ . In the top panel, we compare the dynamic response  $T\chi(C, t_w = 2^{30})$  with the equilibrium curve  $S(C, L = 32)$ . The range of  $C$  covers the peak width of  $P(q, L = 32)$  [7]. Since the curvature is clearly larger for  $T\chi$  than for  $S(C, L = 32)$ , Eq. (H1) tells us that the maximum of  $P_{\text{dyn}}(q; t_w = 2^{30})$  is higher than the maximum of  $P(q, L = 32)$ . The lines correspond to diagonal fits to fourth order polynomials in  $C$  (we increased the order of the polynomial until the figure of merit diagonal- $\chi^2$  for the fit of the dynamic response no longer decreased). The bottom panel shows the second derivative of the interpolating polynomials of the top panel, multiplied by  $-1/2$ . According to Eq. (H1), these derivatives should give us  $P_{\text{dyn}}(q, t_w)$  and  $P(q, L)$ . Indeed, the peak position and height in  $P(q, L = 32)$  is very reasonably reproduced by this approach, see Ref. [7].

response. One can define the *dynamic overlap* probability density function:

$$P_{\text{dyn}}(q; t_w) = -\frac{1}{2} \left. \frac{\partial^2 T\chi(C, t_w)}{\partial C^2} \right|_{C=q}. \quad (\text{H1})$$

Then, one could compare  $P_{\text{dyn}}$  with the equilibrium  $P(q, L)$  at  $q = C(t + t_w, t_w)$ . The weak point in this approach is that taking two derivatives of the curve  $T\chi(C, t_w)$ , which is subject to random errors, is very difficult.

Our way out will be to recall that the area under the peak of the  $P(q, L)$  is approximately  $L$ -independent [7]. Therefore, we shall estimate the peak height (rather than the peak width).

Our efforts to locate the maximum (let alone the full curve) for  $P_{\text{dyn}}(q; t_w = 2^{30})$  are documented in Fig. 14 (but the reader is warned to take the results *cum grano salis*). We note from Fig. 14 that the ratio of the height of the maxima for  $t_w = 2^{30}$  and  $L = 32$  is  $\sim 3.6/2.5$ . Therefore, from the scaling of the peak width,  $\propto L^{-B \approx 0.28}$ , we extrapolate

$$L_{\text{eff}} \sim 32 \times (3.6/2.5)^{\frac{1}{B}} \approx 118, \quad (\text{H2})$$

which is certainly larger than our maximum equilibrium size,  $L = 32$ .

### Appendix I: The simplified $S(C, L)$

In the main text, we wondered about the consequences of having at our disposal only a simplified approximation for  $S(C, L)$ :

$$S_{\text{simpl}}(C, L) = \min \left[ S_0(L) - P_0 C^2 - \frac{P_1}{6} C^4, 1 - C \right]. \quad (\text{I1})$$

In the above equation,  $P_0$  and  $P_1$  are  $L$ -independent constants. All the dependence on the system size is in  $S_0(L)$ .

In fact,  $S_0(L)$  was obtained by fitting the actual data  $S(C = 0, L = 8, 12, 16, 24, 32)$  to a quadratic polynomial in  $L^{-\theta}$ . We took  $\theta = 0.38$  from Ref. [7] [recall that the maximum of the spin-overlap probability,  $P(q, L)$  scales with  $L$  as  $q_{\text{EA}}^{(L)} - q_{\text{EA}}^{(\infty)} \propto L^{-\theta}$ ]. Once  $S_0(L)$  was known, we determined the constants  $P_0$  and  $P_1$  from a least-squares minimization of the difference between  $S_{\text{simpl}}(C, L)$  and the actual data.

- 
- [1] A. Cavagna, Physics Reports **476**, 51 (2009), arXiv:0903.4264.
  - [2] E. Vincent, J. Hammann, M. Ocio, J.-P. Bouchaud, and L. F. Cugliandolo, in *Complex Behavior of Glassy Systems*, Lecture Notes in Physics No. 492, edited by M. Rubí and C. Pérez-Vicente (Springer, 1997).
  - [3] G. F. Rodriguez, G. G. Kenning, and R. Orbach, Phys. Rev. Lett. **91**, 037203 (2003).
  - [4] V. Dupuis, F. Bert, J.-P. Bouchaud, J. Hammann, F. Ladieu, D. Parker, and E. Vincent, Pramana J. of Phys. **64**, 1109 (2005).
  - [5] A. Barrat and L. Berthier, Phys. Rev. Lett. **87**, 087204 (2001).
  - [6] F. Belletti, M. Cotallo, A. Cruz, L. A. Fernandez, A. Gordillo-Guerrero, M. Guidetti, A. Maiorano, F. Mantovani, E. Marinari, V. Martín-Mayor, A. M. Sudupe, D. Navarro, G. Parisi, S. Perez-Gaviro, J. J. Ruiz-Lorenzo, S. F. Schifano, D. Sciretti, A. Tarancon, R. Tripiccion, J. L. Velasco, and D. Yllanes (Janus Collaboration), Phys. Rev. Lett. **101**, 157201 (2008), arXiv:0804.1471.
  - [7] R. A. Baños, A. Cruz, L. A. Fernandez, J. M. Gil-Narvion, A. Gordillo-Guerrero, M. Guidetti, A. Maiorano, F. Mantovani, E. Marinari, V. Martín-Mayor, J. Monforte-Garcia, A. Muñoz Sudupe, D. Navarro, G. Parisi, S. Perez-Gaviro, J. J. Ruiz-Lorenzo, S. F. Schifano, B. Seoane, A. Tarancon, R. Tripiccion, and D. Yllanes (Janus Collaboration), J. Stat. Mech. **2010**, P06026 (2010), arXiv:1003.2569.
  - [8] R. A. Baños, A. Cruz, L. A. Fernandez, J. M. Gil-Narvion, A. Gordillo-Guerrero, M. Guidetti, A. Maiorano, F. Mantovani, E. Marinari, V. Martín-Mayor, J. Monforte-Garcia, A. Muñoz Sudupe, D. Navarro, G. Parisi, S. Perez-Gaviro, J. J. Ruiz-Lorenzo, S. F. Schifano, B. Seoane, A. Tarancon, R. Tripiccion, and D. Yllanes (Janus Collaboration), Phys. Rev. Lett. **105**, 177202 (2010), arXiv:1003.2943.
  - [9] H. Oukris and N. E. Israeloff, Nature Physics **06**, 135 (2010).
  - [10] K. Komatsu, D. L'Hôte, S. Nakamae, V. Mosser, M. Konczykowski, E. Dubois, V. Dupuis, and R. Perzynski, Phys. Rev. Lett. **106**, 150603 (2011), arXiv:1010.4012.
  - [11] L. F. Cugliandolo and J. Kurchan, Phys. Rev. Lett. **71**, 173 (1993).
  - [12] S. Franz and H. Rieger, Journal of Statistical Physics **79**, 749 (1995).
  - [13] E. Marinari, G. Parisi, F. Ricci-Tersenghi, and J. J. Ruiz-Lorenzo, Journal of Physics A: Mathematical and General **31**, 2611 (1998).
  - [14] S. Franz, M. Mézard, G. Parisi, and L. Peliti, Phys. Rev. Lett. **81**, 1758 (1998).
  - [15] S. Franz, M. Mézard, G. Parisi, and L. Peliti, Journal of Statistical Physics **97**, 459 (1999).
  - [16] E. Marinari, G. Parisi, F. Ricci-Tersenghi, and J. J. Ruiz-Lorenzo, J. Phys. A **33**, 2373 (2000).
  - [17] D. Hérisson and M. Ocio, Phys. Rev. Lett. **88**, 257202 (2002), arXiv:cond-mat/0112378.
  - [18] A. Cruz, L. A. Fernández, S. Jiménez, J. J. Ruiz-Lorenzo, and A. Tarancón, Phys. Rev. B **67**, 214425 (2003).
  - [19] D. Hérisson and M. Ocio, Eur. Phys. J. B **40**, 283 (2004), arXiv:cond-mat/0403112.
  - [20] G. Parisi, Phys. Rev. Lett. **43**, 1754 (1979).
  - [21] H. Kawamura, Phys. Rev. Lett. **90**, 237201 (2003).
  - [22] O. V. Billoni, S. A. Cannas, and F. A. Tamarit, Phys. Rev. B **72**, 104407 (2005).
  - [23] G. Parisi, Phys. Rev. Lett. **79**, 3660 (1997).
  - [24] J.-L. Barrat and W. Kob, EPL (Europhysics Letters) **46**, 637 (1999).
  - [25] J.-L. Barrat and L. Berthier, Phys. Rev. E **63**, 012503 (2000).
  - [26] L. Berthier, Phys. Rev. Lett. **98**, 220601 (2007).
  - [27] N. Gnan, C. Maggi, G. Parisi, and F. Sciortino, Phys. Rev. Lett. **110**, 035701 (2013).
  - [28] T. S. Grigera and N. E. Israeloff, Phys. Rev. Lett. **83**, 5038 (1999).
  - [29] L. Bellon, S. Ciliberto, and C. Laroche, EPL (Europhysics Letters) **53**, 511 (2001).
  - [30] C. Maggi, R. Di Leonardo, J. C. Dyre, and G. Ruocco, Phys. Rev. B **81**, 104201 (2010).
  - [31] C. Maggi, R. Di Leonardo, G. Ruocco, and J. C. Dyre, Phys. Rev. Lett. **109**, 097401 (2012).
  - [32] J. R. Gomez-Solano, A. Petrosyan, S. Ciliberto, R. Chetrite, and K. Gawędzki, Phys. Rev. Lett. **103**, 040601 (2009).
  - [33] P. Jop, J. R. Gomez-Solano, A. Petrosyan, and S. Ciliberto, Journal of Statistical Mechanics: Theory and Experiment **2009**, P04012 (2009).
  - [34] N. Greinert, T. Wood, and P. Bartlett, Phys. Rev. Lett. **97**, 265702 (2006).
  - [35] D. Bonn and W. K. Kegel, The Journal of Chemical Physics **118**, 2005 (2003).
  - [36] E. Dieterich, J. Camunas-Soler, M. Ribezzi-Crivellari, U. Seifert, and F. Ritort, Nat Phys **11**, 971 (2015).

- [37] F. Belletti, M. Cotallo, A. Cruz, L. A. Fernandez, A. Gordillo, A. Maiorano, F. Mantovani, E. Marinari, V. Martín-Mayor, A. Muñoz Sudupe, D. Navarro, S. Perez-Gaviro, J. J. Ruiz-Lorenzo, S. F. Schifano, D. Sciretti, A. Tarancon, R. Tripiccone, and J. L. Velasco (Janus Collaboration), *Comp. Phys. Comm.* **178**, 208 (2008), arXiv:0704.3573.
- [38] M. Baity-Jesi, R. A. Baños, A. Cruz, L. A. Fernandez, J. M. Gil-Narvion, A. Gordillo-Guerrero, D. Iniguez, A. Maiorano, F. Mantovani, E. Marinari, V. Martín-Mayor, J. Monforte-Garcia, A. Muñoz Sudupe, D. Navarro, G. Parisi, S. Perez-Gaviro, M. Pivanti, F. Ricci-Tersenghi, J. J. Ruiz-Lorenzo, S. F. Schifano, B. Seoane, A. Tarancon, R. Tripiccone, and D. Yllanes (Janus Collaboration), *Comp. Phys. Comm* **185**, 550 (2014), arXiv:1310.1032.
- [39] K. Gunnarsson, P. Svedlindh, P. Nordblad, L. Lundgren, H. Aruga, and A. Ito, *Phys. Rev. B* **43**, 8199 (1991).
- [40] M. Palassini and S. Caracciolo, *Phys. Rev. Lett.* **82**, 5128 (1999), arXiv:cond-mat/9904246.
- [41] H. G. Ballesteros, A. Cruz, L. A. Fernandez, V. Martín-Mayor, J. Pech, J. J. Ruiz-Lorenzo, A. Tarancon, P. Tellez, C. L. Ullod, and C. Ungil, *Phys. Rev. B* **62**, 14237 (2000), arXiv:cond-mat/0006211.
- [42] Y. G. Joh, R. Orbach, G. G. Wood, J. Hammann, and E. Vincent, *Phys. Rev. Lett.* **82**, 438 (1999).
- [43] F. Bert, V. Dupuis, E. Vincent, J. Hammann, and J.-P. Bouchaud, *Phys. Rev. Lett.* **92**, 167203 (2004).
- [44] L. Berthier, G. Biroli, J.-P. Bouchaud, L. Cipelletti, D. El Masri, D. L'Hôte, F. Ladieu, and M. Pierno, *Science* **310**, 1797 (2005).
- [45] A. P. Young, *Spin Glasses and Random Fields* (World Scientific, Singapore, 1998).
- [46] A. Cruz, J. Pech, A. Tarancon, P. Tellez, C. L. Ullod, and C. Ungil, *Comp. Phys. Comm* **133**, 165 (2001), arXiv:cond-mat/0004080.
- [47] A. T. Ogielski, *Phys. Rev. B* **32**, 7384 (1985).
- [48] F. Belletti, M. Guidetti, A. Maiorano, F. Mantovani, S. F. Schifano, R. Tripiccone, M. Cotallo, S. Perez-Gaviro, D. Sciretti, J. L. Velasco, A. Cruz, D. Navarro, A. Tarancon, L. A. Fernandez, V. Martín-Mayor, A. Muñoz-Sudupe, D. Yllanes, A. Gordillo-Guerrero, J. J. Ruiz-Lorenzo, E. Marinari, G. Parisi, M. Rossi, and G. Zanier (Janus Collaboration), *Computing in Science and Engineering* **11**, 48 (2009).
- [49] F. Belletti, A. Cruz, L. A. Fernandez, A. Gordillo-Guerrero, M. Guidetti, A. Maiorano, F. Mantovani, E. Marinari, V. Martín-Mayor, J. Monforte, A. Muñoz Sudupe, D. Navarro, G. Parisi, S. Perez-Gaviro, J. J. Ruiz-Lorenzo, S. F. Schifano, D. Sciretti, A. Tarancon, R. Tripiccone, and D. Yllanes (Janus Collaboration), *J. Stat. Phys.* **135**, 1121 (2009), arXiv:0811.2864.
- [50] G. Parisi, F. Ricci-Tersenghi, and J. J. Ruiz-Lorenzo, *Eur. Phys. J.* **11**, 317 (1999), arXiv:cond-mat/9811374.
- [51] F. Ricci-Tersenghi, *Phys. Rev. E* **68**, 065104 (2003).
- [52] L. A. Fernández and V. Martín-Mayor, *Phys. Rev. B* **91**, 174202 (2015).
- [53] M. Manssen, A. K. Hartmann, and A. P. Young, *Phys. Rev. B* **91**, 104430 (2015), arXiv:1501.06760.
- [54] M. Wittmann and A. P. Young, *Journal of Statistical Mechanics: Theory and Experiment* **2016**, 013301 (2016).
- [55] M. Mézard, G. Parisi, and M. Virasoro, *Spin-Glass Theory and Beyond* (World Scientific, Singapore, 1987).
- [56] The reader will note that data for  $t_w = 2^{19}$  are slightly off, in Fig. 3. We attribute the effect to a strong statistical fluctuation, enhanced by the fact that all data points with the same  $t_w$  are extremely correlated.
- [57] Note that the delta peak in Eq. (10) is a reasonable expectation only for an infinite system, cf. Appendix A.
- [58] E. Marinari, G. Parisi, F. Ricci-Tersenghi, J. J. Ruiz-Lorenzo, and F. Zuliani, *J. Stat. Phys.* **98**, 973 (2000), arXiv:cond-mat/9906076.
- [59] M. Lulli, G. Parisi, and A. Pelissetto, *Phys. Rev. E* **93**, 032126 (2016).
- [60] M. Baity-Jesi, R. A. Baños, A. Cruz, L. A. Fernandez, J. M. Gil-Narvion, A. Gordillo-Guerrero, D. Iniguez, A. Maiorano, F. Mantovani, E. Marinari, V. Martín-Mayor, J. Monforte-Garcia, A. Muñoz Sudupe, D. Navarro, G. Parisi, S. Perez-Gaviro, M. Pivanti, F. Ricci-Tersenghi, J. J. Ruiz-Lorenzo, S. F. Schifano, B. Seoane, A. Tarancon, R. Tripiccone, and D. Yllanes (Janus Collaboration), *Phys. Rev. B* **88**, 224416 (2013), arXiv:1310.2910.
- [61] J. A. Mydosh, *Spin Glasses: an Experimental Introduction* (Taylor and Francis, London, 1993).
- [62] C. Chatelain, *Journal of Physics A: Mathematical and General* **36**, 10739 (2003).
- [63] We do not used the so-called “natural” cubic spline. Instead, we fixed the first and last derivative of the interpolating function from three points of a parabolic fit.